ELSEVIER

Journal of Nuclear Materials 264 (1999) 78–88

journal of nuclear materials

Investigations on Inconel 718 irradiated with 800 MeV protons

F. Carsughi [a,d,*], H. Derz [b], P. Ferguson [c], G. Pott [b], W. Sommer [c], H. Ullmaier [a]

[a] *Institut für Festkörperforschung, Forschungszentrum Jülich, Jülich, Germany*
[b] *Heiße Zellen, Forschungszentrum Jülich, Jülich, Germany*
[c] *APT Technical Project Office, Los Alamos National Laboratory, Los Alamos, USA*
[d] *Facoltà di Agraria, Università degli Studi di Ancona and INFM, UdR Ancona, Via Ranieri 65, I-60131 Ancona, Italy*

Received 8 May 1998; accepted 13 July 1998

Abstract

In spallation sources, the neutrons (utilized as probes for condensed matter research or for inducing nuclear transmutations) are generated by protons of around 1 GeV energy which cause spallation of the nuclei in a heavy metal target. The beam powers of the proposed future facilities are in the range of 1 to several 10 MW and the corresponding high particle fluxes make radiation damage the crucial effect for the lifetime of target structural materials in or close to the proton beam. In order to establish a database on spallation-relevant radiation effects, post-irradiation investigations of components of spent targets from operating medium power sources are being performed. Here we report first results on Inconel 718 irradiated in LAMPF up to a fluence of 3×10^{25} p/m^2. Microhardness and bending tests together with SEM and TEM investigations show a considerable degradation of the mechanical properties of the material requiring additional highly controlled tests, now underway, to determine fracture toughness and tensile properties as a function of dose.

1. Introduction

For several decades fission reactors have been the main source of neutrons used as a versatile probe for condensed matter research, through scattering and spectroscopy measurements. However, the development potential of high flux reactors has reached its limits and it is now established that the next generation of neutron sources will be accelerator-based facilities where the neutrons are produced by high energy protons (≈1 GeV) inducing spallation of the nuclei in a heavy metal target. Spallation sources can relatively easily deliver neutron pulses of lengths in the μs range by imposing a time structure on the proton beam. This not only increases the peak intensities, but also allows time-of-flight measurements providing, for many applications, more efficient use of the neutrons than cw sources. Recognizing these advantages and the successful operation of a few low and medium power (ISIS [1]) pulsed neutron sources, there are worldwide plans to construct high-power spallation sources with beam powers of 1 [1] to 5 MW. Recently completed technical studies for the European Spallation Source (ESS) [3] and the United States Spallation Neutron Source (SNS) [4] have proven their feasibility but have also identified areas where vigorous research and development must go on in order to achieve optimum solutions. Other future applications of spallation sources with even higher beam powers include the transmutation of nuclear waste [5,6] and the production of tritium [7].

In the target region of accelerator driven facilities, radiation damage by the high energy protons and neutrons is considered the most critical load to the target and the structural materials in or close to the proton beam. Since the extensive database on radiation effects in fission and fusion materials can only partly be transferred to the spallation case, there is an urgent need for results obtained (a) with spallation-relevant pro-

[1] The first spallation source approaching a beam power of 1 MW is the continuous source SINQ [2] in PSI-Switzerland (starting operation in December 1996).

* Corresponding author.

0022-3115/99/$ – see front matter
PII: S0022-3115(98)00475-9

ductions of atomic displacements and foreign elements (particularly H and He isotopes) and (b) at the operating temperatures (RT to 300°C) of structural target components [8,9]. Extensive international irradiation programs are therefore under way or planned in the medium-power sources LANSCE (Los Alamos Neutron Science Center) and SINQ (Paul Scherrer Institut, Switzerland). Until the results of these efforts are available, the most valuable source of information on the behavior of materials in a spallation environment are specimens taken from spent targets and components of operating sources. Within an international collaboration target components from ISIS and LANSCE (see Table 1) have been shipped to Jülich for post-irradiation testing. Since the radioactivity of the component is extremely high, all investigations have to be performed in the hot cells of the Forschungszentrum Jülich (FZJ).

In this work we report results on the LANSCE Water Degrader (WD) consisting of two concentric spherical shells made of Inconel 718 and AISI 304 L, respectively. The WD is considered the component with the highest irradiation load in a spallation environment available up to now. The accumulated proton charge of 5.3 Ah (Table 1) corresponds to a displacement dose of ≈10 dpa and a helium content of ≈1400 appm in the region around the beam center. In Section 2 information on material parameters of the Inconel alloy used, irradiation history and specimen preparation is given. Results of γ-spectroscopy measurements, microhardness and bending tests and transmission (TEM), and scanning electron microscopy (SEM) are presented in Section 3. Finally the results are briefly discussed in Section 4.

2. Experimental

2.1. Material

The nickel-base alloy Inconel 718 has a nominal composition of 53% Ni, 18% Cr, 18% Fe, 5% Nb, 3% Mo and 1% Ti. After machining, the following heat treatment was applied to the outer shell of WD: (1) Annealing at 1065°C for 1 h and air cooling, (2) Aging at 760°C for 10 h, (3) then furnace cooling to 650°C at 55°C/h, and (4) Holding at 650°C for a total time of 20 h. After such a heat treatment, the microstructure of Inconel 718 contains fine dispersions of γ'(fcc) and γ''(bct) precipitates. The resulting yield strength is about (1000 ± 100) MPa at room temperature, the total elongation at fracture is 15–20% in tests using ASTM bar specimens and about 12% when miniature sheet specimens are used. Unfortunately, no original material in the nonirradiated state was kept after the WD was installed in the LANSCE facility in 1988. Therefore, Inconel 718 with a similar heat treatment supplied by Maschinen-Turbinen-Union [10] had to be used as reference material.

2.2. Irradiation

The WD was placed between the proton entry window and the isotope production targets in the beam stop area of LANSCE and was used as a neutrino source. The nominal profile of the proton beam at the WD position had a Gaussian shape with a standard deviation σ of about 20 mm and its energy was estimated to 760 MeV. The WD was in operation for 419 days in the period October 1988 to September 1993, traversed by protons with a total charge of 5.3 Ah [11]. An analysis of the recordings of the thermocouples placed on the external surface of the water-cooled WD and heat transfer calculations indicate that the maximum temperature of the material in the beam center did not exceed 250°C. Since it was recognized that the beam position in the vertical direction was not stable during the whole irradiation period, the spatial fluence distribution and the corresponding damage parameters were determined by an analysis of γ-spectroscopy (see Section 3.1).

2.3. Specimen preparation

After shipping the component from Los Alamos to Jülich in Fall 1996, the spherical WD (outer diameter 200 mm) was cut into two halves in the hot cells (HZ) of the Forschungszentrum Jülich. The results presented in this work were obtained from Inconel specimens prepared from the 3.1 mm thick hemispherical outer shell of the WD which faced the proton beam. In a first step,

Table 1
Target and components irradiated with high energy protons at LANSCE and ISIS, shipped to the hot cells of the Forschungszentrum Jülich

Component	Material	Irradiated at	Total charge (Ah)
Water degrader	IN 718 and AISI 304L	LANSCE	5.3
Beam window	IN 718	LANSCE	1.2
PSI window #1	DIN 1.4926	LANSCE	2.5
PSI window #2	DIN 1.4926	LANSCE	2.8
ISIS TA target	Ta and AISI 304L	ISIS	1.7

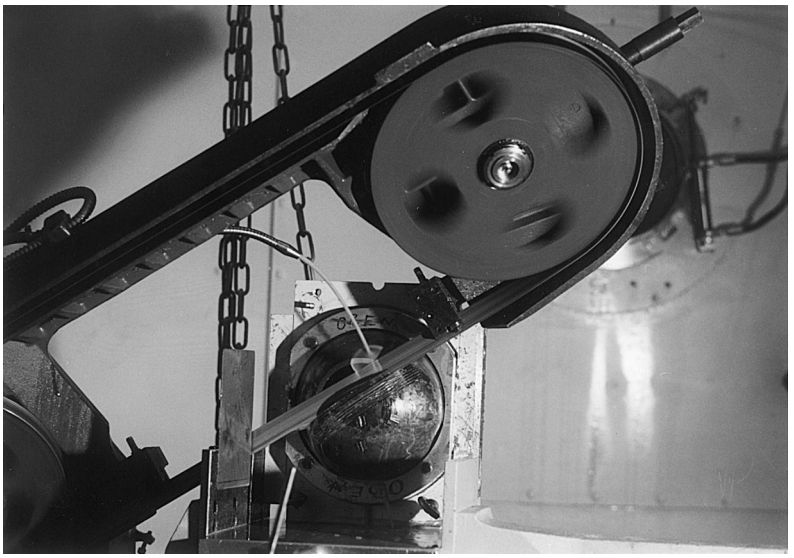

Fig. 1. The WD under the saw while cutting the strips in the hot cells.

strips of 2.1 mm width running through the area hit by the beam were cut by a band saw (see Fig. 1). The measured dose rates of each of the 11 strips (see Fig. 2) reflect the beam profile in the vertical direction y.

A best fit using a Gaussian function allowed the approximate determination of the actual beam center and yielded a standard deviation σ_y of (28 ± 3) mm, i.e. higher than the nominal value of 20 mm which is consistent with the expected unstable position of the beam in the vertical direction.

In a second step the strips with a cross section of 2.1×3.1 mm^2 were selected for investigation with different methods in different laboratories (see Table 2). In the following the results obtained in the HZ Jülich on specimens prepared from strips 4–7 and 11 are reported. The specimen dimensions and positions are given in the respective sections.

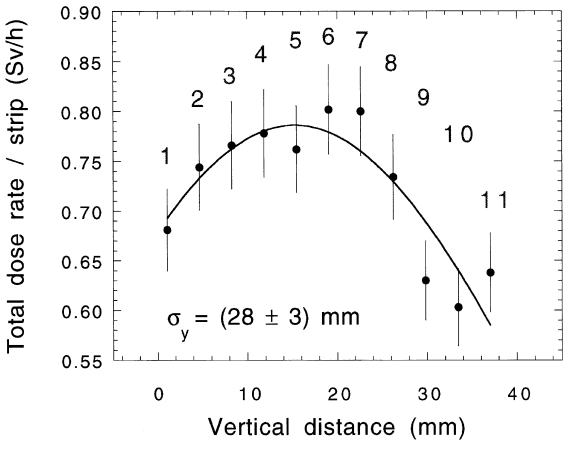

Fig. 2. Overall strip activity as a function of position on the WD. A best fit with a gaussian function is shown as a solid line.

3. Results

3.1. γ-Spectroscopy

After recognizing discrepancies between the nominal and real profile of the proton beam, a device was designed and constructed which allows the precise determination of the beam parameters by γ-spectroscopy. The irradiated component can be translated and rotated such that the area ($\approx 4 \times 7$ mm^2) sampled through a

Table 2
Experimental plan on each strip cut from the outer shell of the LANSCE water degrader made of Inconel 718

Strip	Laboratory	Experimental investigations
1	BNL	*Corrosion test*
2		
3		
4	FZJ	Bending test, TEM, SEM, γ-spectroscopy, *Punch test*
5	FZJ	Bending test, γ-spectroscopy
6	FZJ, ORNL	Bending test, Microhardness, *ABI*
7	FZJ	Microhardness
8		
9	BNL	*Corrosion test*
10	BNL	*Corrosion test*
11	FZJ	Bending test, TEM, SEM, *Punch test*

Tests written in italics are in progress.

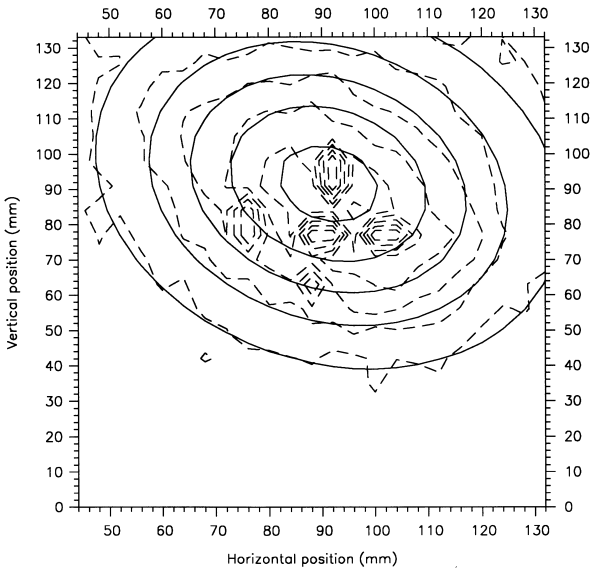

Fig. 3. γ-scan of ^{57}Co the inner shell of the WD made of austenitic steel AISI 304L as a function of the position. The isointensity lines (dashed) and a best fit with a 2D gaussian function (solid lines) are shown. In the geometrical center of the inner shell of the WD 5 holes, for cooling reasons, are visible.

collimator is always perpendicular to the detector of the γ-spectrometer. Since the upstream outer shell made of Inconel had been cut into strips before the γ-scan device was available, the footprint of the beam was determined by using the inner shell (liner) made of AISI 304 L austenistic stainless steel for which isointensity lines of the produced isotope ^{57}Co are shown in Fig. 3. A best fit of the data using a 2D Gaussian function yielded $\sigma_x = (22.6 \pm 0.4)$ mm and $\sigma_y = (28.8 \pm 1.5)$ mm. The first value is close to the nominal width, the latter value is in good agreement with that obtained from the dose rate measurements and confirms the varying position of the beam in the vertical direction. The results of the γ-scan measurements allow an accurate coordination of the strips cut from the Inconel shell of the WD with the actual mean position and width of the proton beam (see Fig. 4).

Another goal of the γ-spectroscopy measurements was a check of the reliability of nuclear codes employed in computations of produced isotopes and their activities, the afterheat, etc. For this purpose the γ-spectra of the most active region (about 2 mSv/h mm^3) of strip # 4 were recorded and converted into absolute activity values by using ^{152}Eu with 4.07×10^8 Bq as standard. The results for the five most active isotopes are listed in Table 3 together with values calculated with the LA-

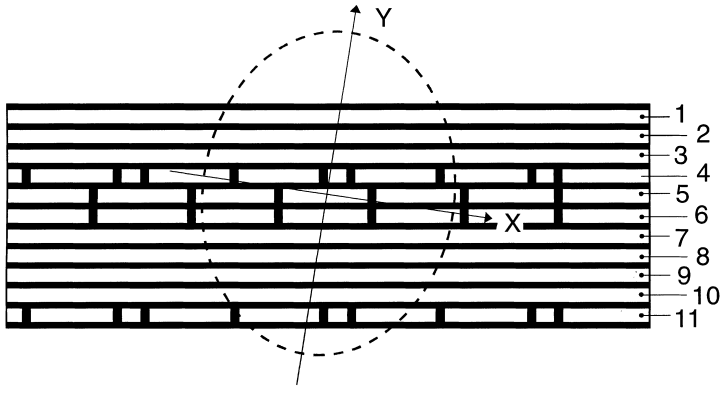

Fig. 4. 11 strips were cut from the Inconel 718 shell of the WD. The actual beam position (as determined by γ scanning, see Fig. 3) is indicated.

Table 3
The five most active isotopes used for the γ-spectroscopy

Isotope	Experimental	Calculated	Calc./Exp.
^{57}Co	6.12×10^9 Bq	1.22×10^{10} Bq	2.0
^{60}Co	1.53×10^8 Bq	1.61×10^8 Bq	1.1
^{54}Mn	3.02×10^9 Bq	3.49×10^9 Bq	1.2
^{22}Na	9.61×10^7 Bq	9.61×10^7 Bq	1.0
^{44}Ti	1.81×10^7 Bq	2.41×10^7 Bq	1.3

Experimental values are compared with those calculated by using LAHET code with the beam parameters described in the text.

HET code [12] for a peak proton fluence of 3×10^{25} p/m^2. This fluence value in the beam center is obtained if the total charge of 5.3 Ah reported by LANSCE (see Table 1) is distributed in a 2D Gaussian beam profile with widths of 22.6 and 28.8 mm, respectively (see above). The comparison of experimental and calculated values shows that the LAHET code seems to overestimate the activities, in the worst case (^{57}Co) by a factor of 2 (see Table 3). The experimental uncertainties were estimated to be about 10%, due to measurement statistics (1%), to standard measurement statistics (4%) and to absorption in the Inconel 718 and standard samples (6%). However, taking into account the long irradiation period with strongly varying production rates and the uncertainties in the fluence determination, the results of the code calculations are considered satisfactory. It may therefore be assumed that the number of displacements of 10 dpa in the region around the beam center calculated by the same code, is a reasonable estimate. This value is supported by calculations using the DIDACS code [13]. The concentration of helium produced by nuclear reactions can be estimated by using experimental numbers [14] to be about 1400 appm in the beam center region.

To this proton-induced damage, the action of fast neutrons created by spallation processes in the WD materials must be added. Estimates show, however, that their contribution is below 2% [15] and is therefore not significant.

3.2. Microhardness

Although microhardness tests do not yield data which are directly applicable for engineering design, they provide valuable information on trends in changes of mechanical properties and require only very small test volumes. This is an important advantage in the present investigation where the volume of material irradiated by high doses is very limited.

Strip # 7 which runs through a region close to the maximum proton flux (see Fig. 2) was therefore used to measure the microhardness as a function of the position along the strip. The strip was embedded in epoxy resin

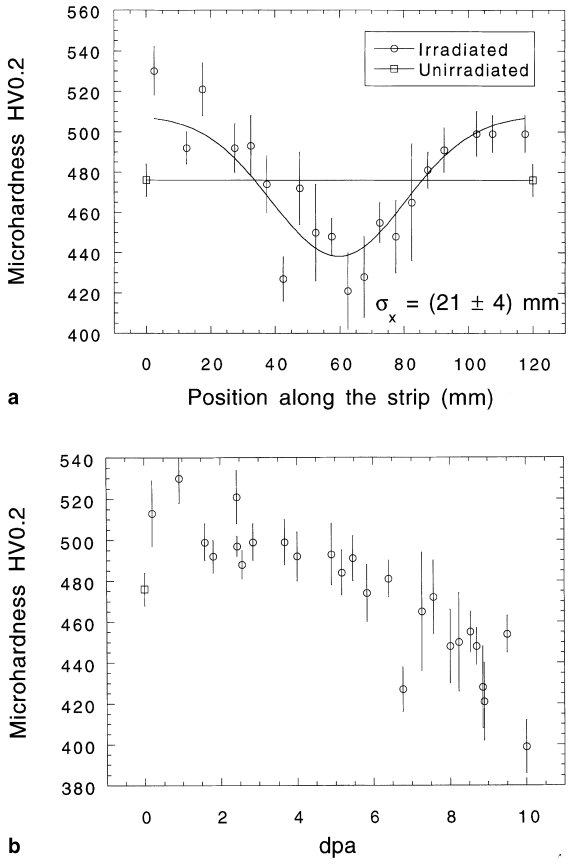

Fig. 5. (a) Microhardness HV0.2 of irradiated Inconel 718 measured along the strip # 7 as a function of the position on the strip (○). A best fit with a gaussian function is shown as a solid line. The reference microhardness value of non-irradiated Inconel 718 is also shown (□). (b) Microhardness HV0.2 of irradiated Inconel 718 as a function of irradiation dose (○). The square gives the value of the non-irradiated reference material.

and polished such that one of the cut flat surfaces (i.e. perpendicular to the spherical surface of the WD) was available for the indentations with the Vickers diamond indentor of the hardness tester. The results of the measurements with a load of 2 N (HV 0.2) at 20 positions along the strip are shown in Fig. 5(a). Each data point is the average of 10 indentations along the thickness. Fitting again a Gaussian function to the variation of HV 0.2 with position x yields a standard deviation $\sigma_x = 21$ mm in excellent agreement with the γ-spectroscopy data on the AISI 304L liner (see Section 3.1). The position in the strip of each indentation area was used to convert the position-dependence of HV to the dose dependence given in Fig. 5(b). At medium and high fluences a softening of the material with increasing dose is evident. At low fluences the comparison with the hardness values measured in the non-irradiated reference material and

limited data on strip positions far away from the proton beam center may suggest a low radiation-induced hardening. This dose dependence of HV is compatible with the results of the bending tests (see next section) and is discussed in Section 4.

3.3. Bending tests

The decision to use bending tests as the main method to characterize the mechanical behavior of the irradiated WD parts had two reasons. Firstly, the machining of a sufficient number of tensile specimens from the curved strips in the HZ turned out to be impracticable and secondly, it was suspected that the irradiation had caused a strong embrittlement of Inconel leading to the problems which are well known in tensile testing of brittle materials such as ceramics.

In order to keep the dose variation in each specimen as small as possible and to obtain a number of specimens which is sufficient for a reasonable statistics and for studying the dose dependence of the mechanical properties, a specimen geometry with an unusual small ratio of length to cross-section (15 mm × 3.1 × 2.1 mm^2) had to be chosen. The small length required a great skill in placing the specimens on the 3-point bending device in the HZ by remote handling. Another disadvantage of the small lengths were the high loads L necessary for bending the specimens to failure. The resulting large forces on the supports (two cylinders of 2 mm diameter in a distance $l = 10$ mm) led to indentations in the specimens which increase the apparent deflections measured by the linear-variable differential transformer at the convex side of the specimen by up to 50 mm above its actual value. The 3-point bending device (schematically shown in Fig. 6) was installed in a standard tensile testing machine equipped with a 5000 N load cell. All tests were performed with a crosshead speed of 0.2 mm/min.

In order to investigate possible influences of sample shape and geometry, extensive tests on non-irradiated specimens were carried out before testing irradiated material. Two examples of results of these preparatory measurements are shown in Fig. 7: The data in Fig. 7(a) demonstrate that neither the slight curvature (radius ≈100 mm) nor the mode of loading (L acting on the concave or the flat (cut) surface, respectively) influence the L–s relationship. Fig. 7(b) shows that the maximum load L_{max} scales with bh^2 (b width, h height of the specimen; for an elastic–ideal plastic material L_{max} would be proportional to bh^2). This empiric scaling was used for normalizing the results of specimens with slightly different dimensions to the nominal values of $h = 3.1$ and $b = 2.1$ mm.

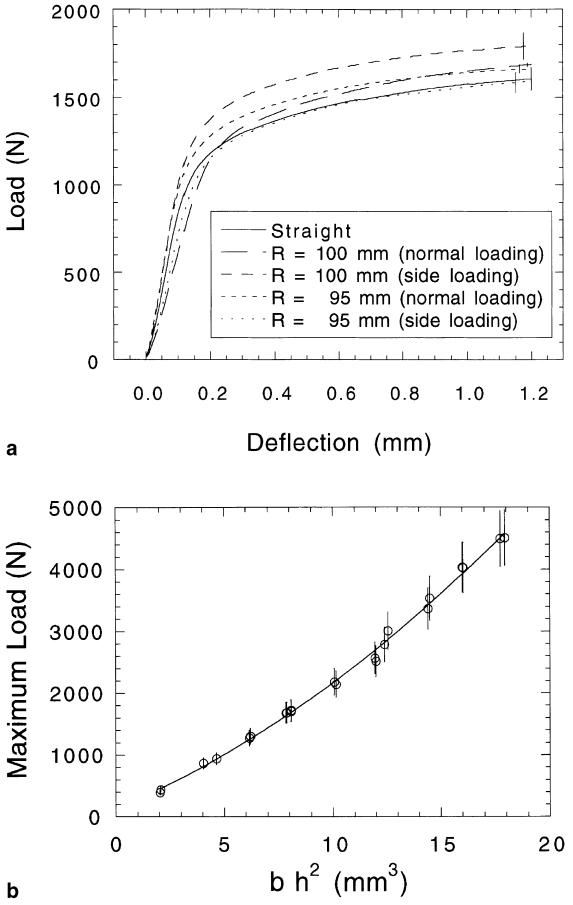

Fig. 7. (a) 3-point bending curves of non-irradiated reference Inconel 718. Specimens with $b = 2$ mm and $h = 2$ mm. In order to check the effect of different sample geometry and loading, one straight and two curved samples, with curvature radii $R = 95$ and 100 mm, were considered, for side and normal loading geometry, respectively. Errors are estimated by averaging different curves and reported only on one point, for clarity. (b) Maximum loads of bending tests on non-irradiated Inconel 718 samples with different widths b and heights h, as a function of bh^2. A best fit with a parabolic function is also shown.

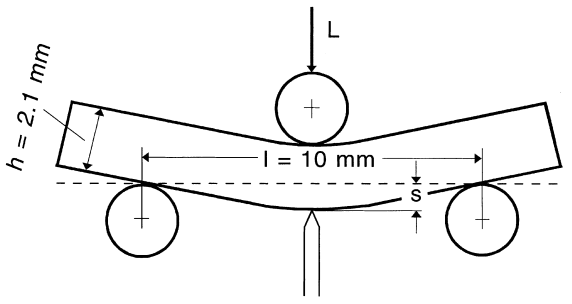

Fig. 6. Schematic view of the 3-point bending device with load L and deflection s.

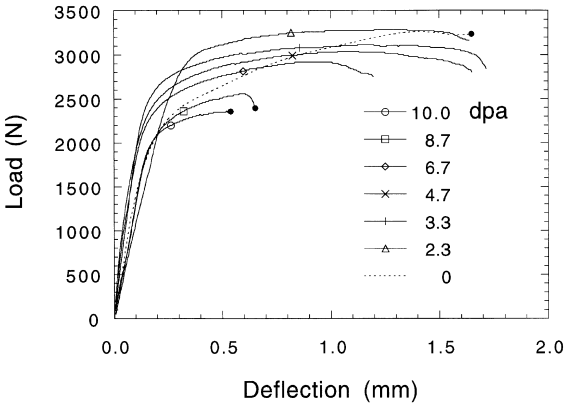

Fig. 8. 3-point bending curves of irradiated Inconel 718 samples obtained from strip #4. The non-irradiated reference curve was normalized as described in the text. In the cases of sample failure, the rupture point is indicated.

The results of bending tests on irradiated Inconel 718 reported here were obtained with specimens cut from strip # 4 (see Fig. 4). The load–deflection curves for the six specimens are shown in Fig. 8 together with the corresponding normalized curve for the non-irradiated reference material. The change in the load as a function of dose is in qualitative agreement with the microhardness results: hardening at low doses and softening at high doses. The deflection to failure changes little at low doses but decreases substantially at high doses. This loss in ductility is connected with a transition from a transgranular fracture mode at low doses to an intergranular failure at high doses (see Section 3.4).

An attempt to extract standard tensile parameters (yield stress, ultimate tensile strength) from the bending test data is under way by using Finite Element (FE) calculations. Their results together with planned ball punch tests and their FE analysis will be reported elsewhere.

3.4. Scanning electron microscopy

The fracture surfaces of the specimens bent to failure were characterized by observation in a SEM located in the HZ-area. Three typical micrographs are shown in Fig. 9. Transgranular ductile failure was observed for the reference material (see Fig. 9(a)) and this failure mode partially persisted for the irradiated specimens up to doses of about 8 dpa. Above this value a mixed fracture mode appeared (see Fig. 9(b)) and became fully intergranular at the highest dose of 10 dpa (see Fig. 9(c)). This rather abrupt change in the fracture

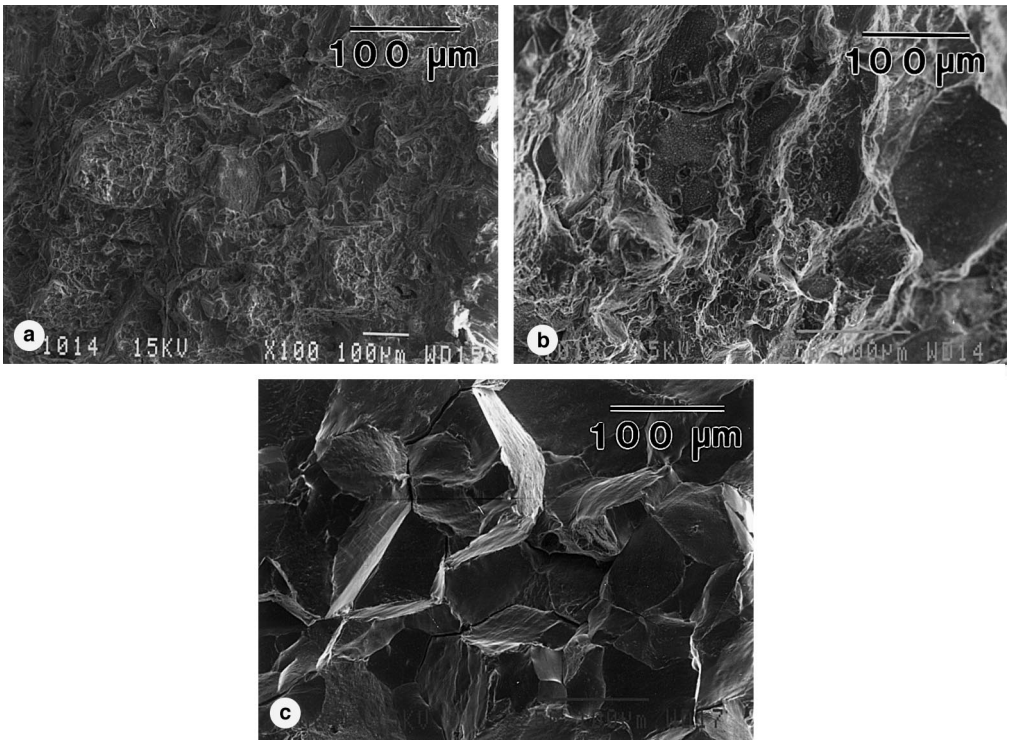

Fig. 9. Scanning electron micrographs of the fractured area of bent samples exposed to: (a) 0.8×10^{25} p/m^2, which corresponds to about 2.5 dpa; (b) 2.6×10^{25} p/m^2, which corresponds to about 8.5 dpa; (c) 3.0×10^{25} p/m^2, which corresponds to about 10 dpa.

mode at high doses is consistent with the results of the bending test which exhibit only moderate reductions in the deflections to failure for low and medium doses whereas the ductility is substantially decreased for the two specimens irradiated to the highest dose levels (see Fig. 8).

Several non-irradiated specimens and specimens irradiated to low and medium doses did not fail within the achievable range of deflections (up to about 1.8 mm) of the bending device. SEM observation of the lower (tensile loaded) surface of such ductile non-irradiated specimens revealed microcracks at deflections above the maximum load. Their presence makes a FE analysis of the bending curves at high deflections very difficult.

3.5. Transmission electron microscopy

Radiation-induced changes in the microstructure were investigated by TEM on non-irradiated reference material and on specimens from areas of maximum proton fluence. The TEM specimens were prepared by mechanically polishing disks of 2.3 mm diameter down to about 80 μm, thereby reducing the activity of the irradiated materials to acceptable values for TEM work. The final thinning was achieved by electropolishing with an electrolite of 5% perchloric acid in ethanol at −20°C. The observations were performed in a EM-430 Philips microscope operated at 300 KeV.

The investigation of the reference material revealed a microstructure which is fully consistent with published results [16,17] and shows fine dispersions of ordered $L1_2$ fcc γ' and ordered DO_{22} bct γ'' phases as the most important features. In the grain boundaries large carbides precipitates are present.

In the material irradiated to 3×10^{25} p/m^2 (≈10 dpa), most of the intergranular precipitates have disappeared. Irradiation also induces drastic changes in the matrix precipitate structure as illustrated in Fig. 10. In the non-irradiated material, the forbidden 100 spots are visible due to the ordered structure of the precipitated phases, while after irradiation those spots have disappeared and streaks in the ⟨1 1 1⟩ direction of the γ matrix are found. This experimental evidence is consistent with a platelet-like shape of the new precipitates which are found to habit the {1 1 1} γ matrix. This can be shown by analyzing the diffraction patterns of different γ matrix planes, such as the {0 0 1}, {$\bar{1}$ 1 4} and {$\bar{1}$ 1 2} planes which are shown in Fig. 11, together with an intermediate position between the {0 0 1} and the {−1 1 4} pattern.

While tilting the sample, the 200 diffraction spot of the {0 0 1} pattern splits into four spots and they move all the way to the spot 3$\bar{1}$1 of the {1 1 4} pattern and further to the spot 1$\bar{1}$2 of the {1 1 2} pattern. This shows that the streaks move on the crystallographic direction ⟨1 1 1⟩ and that the platelet-like precipitates habit the {1 1 1} γ matrix plane. By using {1 1 1} γ matrix plane diffraction patterns, the new precipitates were unambiguously identified as η phase, which has a hexagonal structure and it is found in the non-irradiated superalloy as an overaged product. The {0 0 0 1} basal planes of the hexagonal structure lie on the {1 1 1} planes of the γ matrix.

Similar results were found in Inconel 718 after irradiation with 5 MeV Ni ions [18] and with fast neutrons [19].

4. Discussion and conclusions

The post-irradiation tests reported in Sections 2 and 3 yield the first high-dose mechanical properties data for a component exposed to a radiation environment which is typical for spallation targets. Programmatic urgencies required that the initial measurements be made in a short time frame. Although this meant that far-from-ideal specimen geometries had to be used, very useful data on the lifetime of components in future high-power sources could be obtained. The investigated nickel-base alloy Inconel 718 is a candidate material for water-cooled structural components of spallation targets because of its high strength and corrosion resistance. Its yield strength of about 1 GPa is considerably higher than that of stainless steels and is mainly due to a high density of γ' and γ'' precipitates. For this optimized microstructure, radiation-induced additional obstacles for dislocation movement have obviously only a minor effect which is indicated by the small hardness increase observed at low doses (see Fig. 5(b)). At medium and high doses, the hardness continuously decreases and falls below the initial value at doses of about 6 dpa. This softening may be explained by the radiation-induced dissolution of the original precipitates (see Fig. 10) and the appearence of the η precipitates. These particles are also found in the overaged state of Inconel 718 and are apparently less efficient dislocation barriers which results in the observed reduced strength of both the overaged and the high-dose irradiated (see Figs. 5 and 8) alloys.

A loss in strength is usually accompanied by an increase in ductility. In the irradiated Inconel 718 this is not the case. The bending tests (see Fig. 8) show a substantial decrease of the deflection to failure for doses higher than about 7 dpa. This loss in ductility is connected with a change of the fracture mode from transgranular to mixed to intergranular (see Fig. 9(a)–(c)). The cause for this transition is not yet clear. Considering the high concentration of helium (≈1400 appm for the highest dose), it is tempting to assign the weakening of the grain boundaries to helium embrittlement. This effect is, however, a typical high temperature phenomenon [20] observed at temperatures above 0.4 T_m (T_m is the

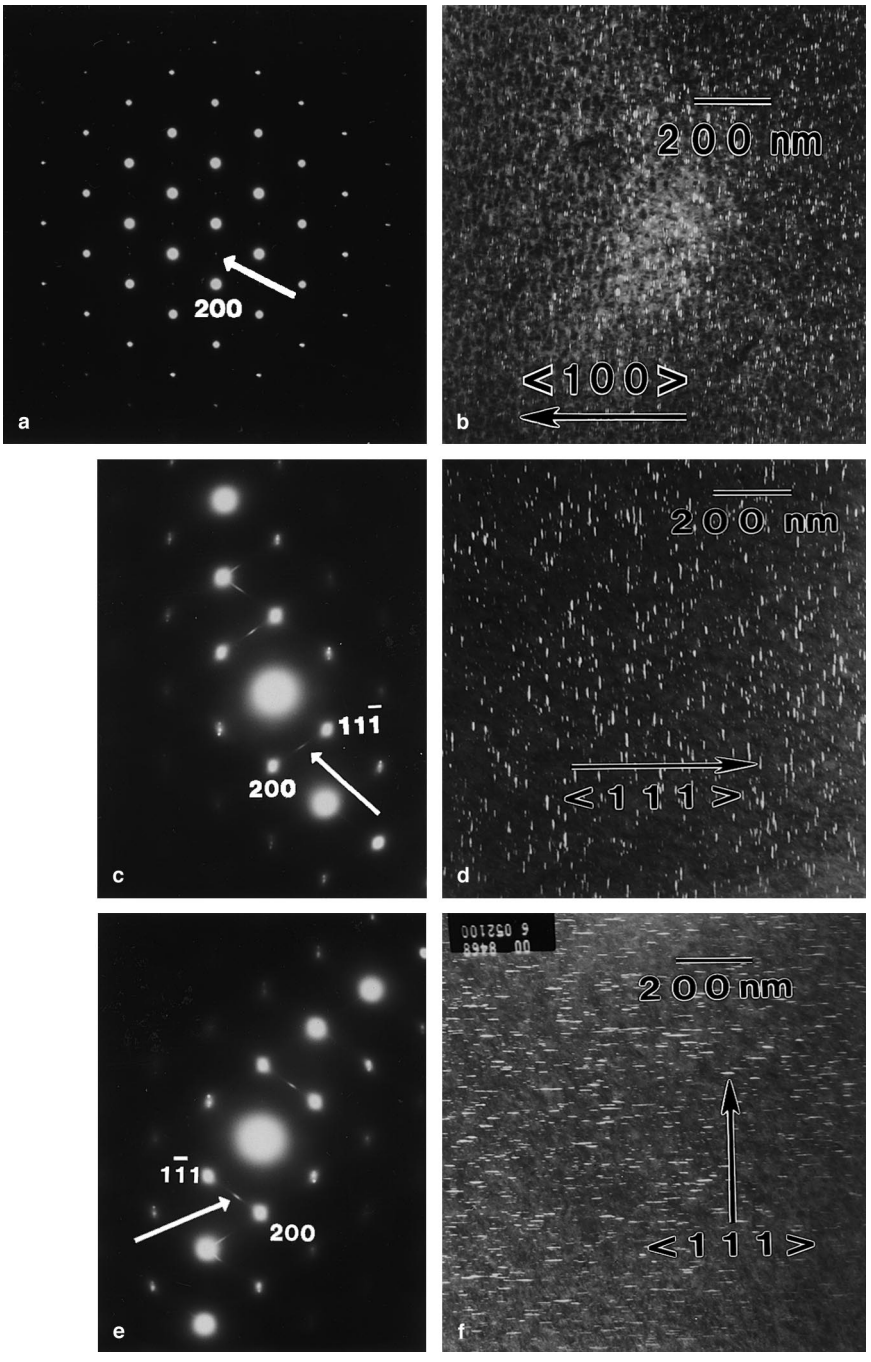

Fig. 10. TEM diffraction patterns of the {0 1 1} γ matrix plane and related dark field images of fully heat treated Inconel 718 non-irradiated and irradiated up to about 10 dpa. The dark field images are taken from the spot indicated by the arrow. *Non-irradiated material*: the {0 1 1} diffraction pattern with the visible 100 superlattice reflections (a) and related dark field image (b) are shown; the ⟨1 0 0⟩ crystallographic direction of the γ matrix is also reported. *Irradiated material*: the {0 1 1} diffraction patterns do not show signs of the 100 superlattice reflections, but streaks induced by the irradiation are present (c and e). Dark field images related to the radiation-induced streaks show that the precipitates are perpendicular to the ⟨1 1 1⟩ crystallographic direction of the γ matrix (d and f).

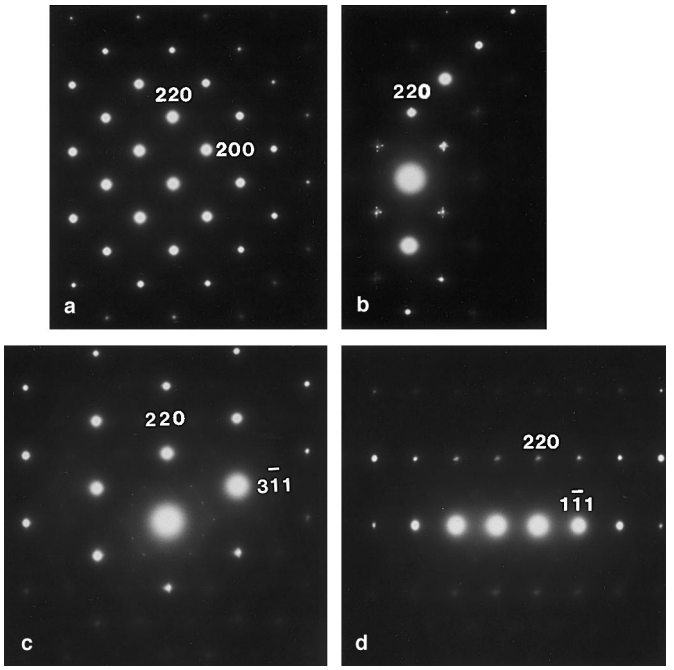

Fig. 11. Tilting angle dependence of TEM diffraction patterns of the fully heat treated Inconel 718 irradiated up to about 10 dpa. (a) The {0 0 1} diffraction pattern (tilting angle = 0°). (b) An intermediate diffraction pattern between the {0 0 1} and {$\bar{1}$ 1 4} ones (tilting angle = −8°). (c) The {$\bar{1}$ 1 4} diffraction pattern (tilting angle = −19°). (d) The {$\bar{1}$ 1 2} diffraction pattern (tilting angle = −30°).

melting temperature) where He atoms become mobile and form bubbles. Moreover, simulation experiments on austenitic and martensitic steels [21] indicate that He-concentrations up to 5000 appm have little influence on the mechanical properties of these materials in the temperature range of 20–300°C. Alternative explanations for the observed intergranular embrittlement of Inconel 718 are radiation-induced segregation of compositional elements and/or transmutation-induced elements at the grain boundaries or the formation of the η phase. TEM studies are planned to uncover the dominating embrittlement mechanism.

Besides strength, the fracture toughness K_c of a material is of utmost importance for its use in a component which has to withstand high mechanical loads. Since K_c values cannot be extracted from the present experimental data, we use the area AML under the load–deflection curves (see Fig. 8) up to the maximum loads as a qualitative measure of the toughness. AML has the dimension of an energy and decreases with increasing irradiation dose (see Fig. 12). Beyond about 7 dpa (where also the transition in the fracture mode occurs), AML drops to a level which is about 1/5 of that for the non-irradiated material.

This low value infers a strongly reduced resistance against crack propagation and could explain a recent experience at LANSCE where a crack appeared in an Inconel 718 proton window at a dose of about 13 dpa. Examination of data from previous work suggests that a microcrack caused by spot welding a thermocouple to the window surface started to propagate through the thickness of the window material and led to a small water leak [22]. This water leak did not cause a suspension of operations. The window remained in place until operations were completed in June 1997 at which time a damage level of about 22 dpa had been reached. Plans to study the window are now being developed.

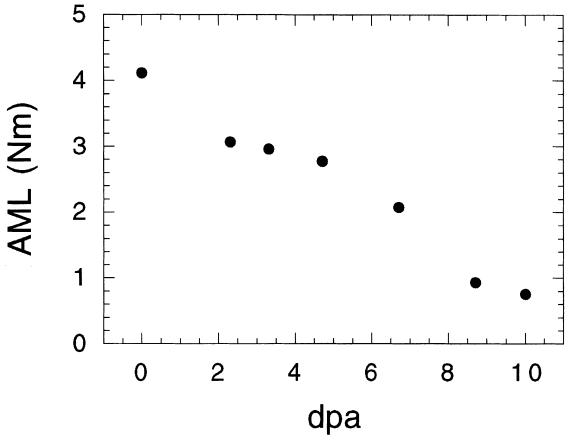

Fig. 12. Area under the load–deflection curve up to the maximum load (AML) as a function of dose of the bending tests.

In the beam centers of ESS and SNS, full power operation time produces 60 and 20 dpa per full-power year, respectively [3,4]. In the APT, operation is scheduled for 75% of each year; the window will reach about 16 dpa and some structural components in the target assembly will reach 35 dpa. Components in the APT require the high-strength available from an alloy such as Inconel 718. In order to establish the mechanical properties response to high energy protons, samples suitable for determining mechanical properties such as strength, ductility, and toughness have been irradiated to doses approaching 15 dpa in the LANSCE facility, and even higher dose irradiations will begin in this year. Initial data from the specimens available now are expected in late-summer 1998.

Experience from fission and fusion materials research and preliminary results on AISI 304L and 1.4926 steel (see Table 1) suggest that alloys with a less radiation-sensitive microstructure should exhibit a considerably higher lifetime. In order to confirm this expectation and establish a database for an optimum materials selection, extensive collaborative programs have been initiated in conjunction with the US-Accelerator Production of Tritium (APT), the European Spallation Source (ESS) and the US-Spallation Neutron Source (SNS). The efforts include irradiations in LANSCE (LANL), SINQ (PSI) and simulation experiments at Forschungszentrum Jülich and Oak Ridge National Laboratory.

Acknowledgements

The authors are grateful to all the staff members of the Hot Cells of the Forschungszentrum Jülich for the effort put in this work. Dr W. Kesternich is also acknowledged for useful discussion on TEM observations. Moreover, we acknowledge the extensive work in preparing the shipment of the radioactive components by M. Zaslawsky and J. Roberts at Los Alamos National Laboratory. We thank Drs M. Louthan and Poh-Sang Lam from the Savannah River Technology Center and Dr H. Cords from FZJ for many helpful discussions regarding the interpretation of our mechanical test results.

References

[1] ISIS 97, The Rutherford Appleton Laboratory, ISIS Facility Annual Report 1996–1997, CLRC (1997).
[2] G.S. Bauer, The Spallation Neutron Source SINQ, Paul Scherrer Institut, CH-5232 Villigen PSI (1994).
[3] ESS – A next generation neutron source for Europe, vol. III: The Technical Study, ESS Council, I. Kjems, Chairman, 1997, ISBN 090 237 6 500 and 090 237 6 659.
[4] Review of the National Spallation Neutron Source Project, US Dept. of Energy, DOE Report DOE/ER-0705 (1997).
[5] For a recent review see C.D. Bowman, in: Proc. Topical Meeting on Nuclear Applications of Accelerator Technology, Albuquerque, NM, 16–20 November 1997, American Nuclear Society, Rep. No. 700 249.
[6] C. Rubbia, S. Bruno, Y. Kadi, J.A. Rubio, European Organ. for Nuclear Res., Report CERN/LHC/97-01 (EET) (1997).
[7] APT Conceptual Design Report, Los Alamos National Laboratory Report LA-UR-97-1329 (1997).
[8] H. Ullmaier, F. Carsughi, Nucl. Instr. and Meth. B 101 (1995) 406.
[9] Proc. of the Intern. Workshops on Spallation Materials Technology: (1) L.K. Mansur, H. Ullmaier (Eds.), ORNL Report CONF-9604151, Oak Ridge, TN, 23–25 April 1996; (2) F. Carsughi et al. (Eds.), FZJ Report JÜL-3450, ISSN 0944-2952, Ancona, Italy, 19–22 September 1997; (3) W. Sommer, L. Daemen, Materials for spallation neutron sources, Los Alamos National Laboratory Report LA-13097-MS (1996); (4) S.A. Maloy et al., Progress Report on the Accelerator Production of Tritium Materials Irradiation Program, published in: Materials for Spallation Neutron Sources, The Minerals, Metals and Materials Society, 1998, p. 131.
[10] W.G. Smarsly, Maschinen-u. Turbinen Union, private communication.
[11] Analysis of LANSCE-Irradiated Beam Entry Windows, Los Alamos National Laboratory, Report LA-UR-95-3376 (1995), data from Los Alamos Neutron Science Center Operations Records.
[12] R.E. Prael, H. Lichtenstein, User Guide to the LCS: The LAHET Code System, Los Alamos National Laboratory, Report LA-UR-89-3014 (1989).
[13] A.Yu. Konobeyev, Yu.A. Korovin, J. Nucl. Mater. 195 (1992) 286.
[14] S.L. Green, W.V. Green, F.H. Hegedus, M. Victoria, W.F. Sommer, B.M. Oliver, J. Nucl. Mater. 155–157 (1988) 1350.
[15] W.F. Sommer, P.D. Ferguson, R.D. Brown, C.M. Cedilo, E. Zimmermann, Experience at the Los Alamos Meson Physics Facility with the use of alloy Inconel 718 as an enclosure for a Beam Degrader and as a proton beam entry window, Los Alamos National Laboratory Report LA-UR-94-2809 (1994).
[16] Kirman, D.H. Warrington, J. Iron Steel Inst. 1264 (1967).
[17] D.F. Paulonis, J.M. Oblak, D.S. Duvall, Trans. ASM 62 (1969) 611.
[18] W.L. Bell, T. Lauritzen, E.S. Darlin, R.W. Warner, in: Irradiation Effects on the Microstructure and Properties of Metals, ASTM STP, vol. 611, 1976, p. 353.
[19] W.L. Bell, T. Lauritzen, in: Effects of Radiation on Materials, 11th Conference, ASTM STP, vol. 782, 1982, p. 139.
[20] H. Ullmaier, H. Trinkaus, Mater. Sci. Forum 97–99 (1992) 451.
[21] H. Ullmaier, E. Camus, J. Nucl. Mater. 251 (1997) 262.
[22] W.F. Sommer, unpublished.